Proceedings of the 34th European Modeling & Simulation Symposium (EMSS), 017
19th International Multidisciplinary Modeling & Simulation Multiconference

ISSN 2724-0029 © 2022 The Authors.
doi: 10.46354/i3m.2022.emss.017

Numerical modelling of aluminothermic reduction for low-carbon-footprint silicon production

Sergey Semenov [1*], Raphaël Bayle[1] and Patrick Namy[1]

[1]SIMTEC, 5 Rue Felix Poulat, Grenoble, 38000, France

[*]Corresponding author. Email address: sergey.semenov@simtecsolution.fr

Abstract

Silicon production usually employs carbon to reduce quartz. A new process using secondary aluminium instead of carbon, and, thus avoiding producing carbon dioxide, is currently being studied. Two immiscible phases are involved in the process, a metal phase, initially composed of aluminium, and a slag phase, initially composed of a mix of lime and quartz. Present numerical work studies different phenomena that contribute to the reaction kinetics, namely diffusion, soluto-gravitational convection and thermo-soluto-gravitational convection. The impact of forced convection on the global reaction rate is also studied. For this purpose, two numerical models, including chemical, thermal and fluid dynamics aspects, are developed: a model where the metal-slag interface is fixed and explicitly represented and a diffuse interface model. The models are numerically solved using the finite element method within the software COMSOL Multiphysics®. The proposed methodology is totally new due to modelling of all physical phenomena in a fully coupled way. The aim of this work is to gain insight into the phenomena contributing to the global reaction rate, which is a critical parameter to control in the silicon production process. The novelty of approach consists in assessing the impact of individual phenomena by incrementing progressively the complexity of models.

Keywords: Silicon production; multiphase CFD; COMSOL Multiphysics; numerical modeling; aluminothermic reduction

1. Introduction

Silicon is a strategic material for European industries and its production is of major interest for many countries. In classical industrial processes to produce silicon, quartz is reduced with carbon as a reductant in submerged arc furnaces (SAF) (Jiang, et al., 2021). The aluminothermic reduction appears to be a more environmentally friendly option as it does not consume raw carbon materials and thus reduces CO_2 emissions. In this work, carried out in the framework of the European project SisAl Pilot, this aluminothermic reduction approach is studied in order to produce decarbonated silicon and to recycle aluminium from aluminium dross and scrap.

The aluminothermic reduction involves two immiscible phases: a metal phase and a slag phase (Park, Sridhar, & Fruehan, 2014). The metal and slag phases are initially pure aluminium and a mix of CaO and SiO_2, respectively. As the reaction proceeds at the interface of these two immiscible phases, the metal and slag are getting enriched with Si and Al_2O_3, respectively.

In the industrial-scale pilot experiment of the SisAl Pilot project, a two-step metallurgical process is planned to be implemented: in the first step, the metal and slag are melted in separate furnaces; in the second one, they are mixed so that they can react.

In the process, heat transfer modelling is critical: aluminothermic reduction is exothermic and contributes to the heating of the metal-slag system as soon as the reaction has started. On one hand, this heating can be dangerous, as local temperature rise can damage the crucible; on the other hand it can be beneficial, as it helps to keep the system in a molten state and to prevent its solidification. The total power of the exothermic heat source is directly defined by the reaction rate (Park, Sridhar, & Fruehan, 2014). Thus, it

is important to understand what defines the global reaction rate, and how to control it in order to stay in an optimal temperature range.

The final composition of the metal and slag phases is another important indicator of the process efficiency. The goal of the process is to maximize the silicon output. Theoretically, the equilibrium composition of phases is defined by the kinetics of aluminothermic reduction that takes place at the interface between immiscible metal and slag phases. However, the time to reach the equilibrium in a whole system depends also on how quickly chemical species are transported across the phases bulk. Both the reaction kinetics and the transport of chemical species, such as diffusion and convection, define the global reaction rate and indicate the required duration of this process to reach a certain phases composition. The intensity of natural convection depends on the liquid layer stability in the Earth's gravitational field (Doering, 2020).

The modelling developed in this work aims at understanding the temperature and composition evolution in the system. More specifically the kinetics of reaction is studied and the impact of modelling hypotheses and considered phenomena is investigated.

Section 2 presents the state of the art in the field of silicon reduction and its numerical modelling. Section 3 describes the numerical methodology and the models that are developed in this work to study the process of aluminothermic reduction of quartz. Section 4 presents and discusses the results of numerical simulations. Conclusions are provided in Section 5. Some aspects of the volume averaging theory are given in Appendix A.

2. State of the art

The reduction of quartz or silica by aluminium has been studied in various contexts, such as rapid bulk reaction during reduction under vacuum conditions (Prabriputaloong & Piggot, 1973), solid state reaction between aluminium and oxidised silicon (Roberts & Dobson, 1984), production of solar grade silicon and electronic grade silicon for photovoltaic applications (Pizzini, 1984), synthesis of coatings (Talako, Yakovleva, Astakhov, & Letsko, 2018), fabrication of porous Si (Mishra, et al., 2018; Gao, et al., 2019) and nano-Si anode materials (Fang, Zhao, Wang, Hu, & Zheng, 2020) for the high-performance Li-ion batteries via the low temperature aluminothermic reduction, construction of new composite materials (Liu, et al., 2021) including *in situ* reduction in powder metallurgy (Deqing & Ziyuan, 2001).

Aluminothermic reduction of silica mostly appears in literature as an experimental research. To the best of authors knowledge, there are no publications dedicated to a direct numerical simulation of such chemical reaction in a metallurgical process. Only distantly related numerical works can be found. One of them uses a molecular dynamics simulation to study the thermite reaction in the $Al\text{-}SiO_2$ sandwich nanostructure (Zhang, Si, Leng, & Yang, 2016).

For other metallurgical processes, however, such as steelmaking, there are lots of numerical studies in the literature, see for example (Tkadleckova, 2021). Also, optimization of metallurgical production systems, not related to silicon industry, can be found in previous I3M conference proceedings (Ramaekers, Pollaris, & Claes, 2014; Bruzzone, Sinelshikov, Cepolina, Giovannetti, & Pernas, 2021).

Experimental studies report that, as the aluminothermic reduction occurs at the interface between the metal and the slag, the chemical equilibrium can be assumed to be reached instantaneously at the interface (Park, Sridhar, & Fruehan, 2014). Recently, the experimental studies carried out in the framework of the SisAl Pilot project have also confirmed a rapid kinetics of the aluminothermic reduction of silica in a metallurgical process (Philipsson, Wallin, Einarsrud, & Tranell, 2021). With the hypothesis of an instantaneous chemical equilibrium at the interface, the global reaction rate is not limited by the kinetics of reaction but by transport mechanisms, such as diffusion and convection, which brought the reactants up to the metal-slag interface and the products of the reaction far from this interface. The numerical values of diffusion coefficients of the substances reacting in the metal and the slag are difficult to find or measure directly. In present numerical study they are computed by extrapolation (Du, et al., 2003) or by magnitude estimations (Amini, 2005).

In the considered system, slag and metal are two immiscible phases, thus it is necessary to consider a two-phase model. In computational fluid dynamics, there exists a number of numerical approaches to model moving boundaries and interfaces in multi-phase systems, such as interface tracking (marker-and-cell, front-tracking) and interface capturing methods (volume of fluid, level set, phase field), see for example an overview of methods in (Mirjalili, Jain, & Dodd, 2017). Since interfacial tension phenomena are not studied in present work, a simpler volume averaging approach (Whitaker, 1985; Drew & Passman, 1999) seems to be the most suitable and computationally less expensive method for the present study. Volume averaging method makes it possible to implicitly represent interfaces between two immiscible phases by using one continuous field. In this case the interfaces are said to be diffuse, that is having a spatially continuous and smooth phase transition across them.

3. Methods and models

3.1. Numerical methods

The numerical resolution of the system of partial differential equations (PDE) is done with the finite element method (FEM), within the software COMSOL

Multiphysics®, versions 5.5. The number of degrees of freedom varies from 36000 for purely diffusive problem up to 777000 for a problem with soluto- and thermo-gravitational convective instabilities.

3.2. Developed models

Two models are studied: in the first model, the interface between metal and slag is well-defined and fixed, in the second model, this interface is defined using a fraction field which provides a diffuse description of the interface and allows it to move.

3.2.1. *Well-defined interface model*

In this section, a model where the geometry of the system is fixed is presented, within the assumption that the total volume of both phases remains constant.

Denoting c_i the concentration field of compound i (with $i = Al,\ Si$ in metal and $i = Al_2O_3, SiO_2$ in slag), $\mathbf{u}_\alpha$ the velocity field in phase α ($\alpha = m, s$ standing for metal and slag phases) and D_i the chemical diffusivity of compound i, the chemical transport equation reads,

$$\frac{\partial c_i}{\partial t} + \nabla \cdot (\mathbf{u}_\alpha c_i - D_i \nabla c_i) = 0$$

Each of those equations is defined exclusively in either the slag or the metal domain, represented in Figure 1.

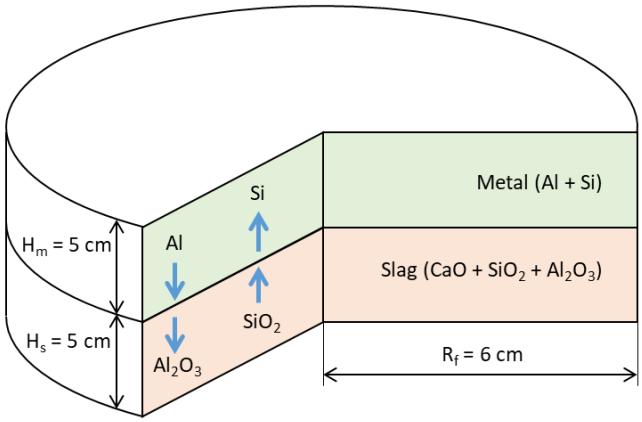

Figure 1. Geometry for the aluminothermic reduction model with well-defined interface between metal and slag phases

In each domain, velocity fields $\mathbf{u}_\alpha$, $\alpha = m, s$, are calculated with the Navier-Stokes equations for incompressible fluid under the Boussinesq approximation,

$$\rho_{\alpha,0}\left(\frac{\partial \mathbf{u}_\alpha}{\partial t} + \mathbf{u}_\alpha \cdot \nabla \mathbf{u}_\alpha\right) = \nabla \cdot \boldsymbol{\sigma}_\alpha + \mathbf{f}_\alpha$$

$$\boldsymbol{\sigma}_\alpha = -\nabla p_\alpha + \mu_\alpha(\nabla \mathbf{u}_\alpha + (\nabla \mathbf{u}_\alpha)^\top)$$

$$\mathbf{f}_\alpha = \big(\rho_\alpha(c_i, T) - \rho_{\alpha,0}\big)\mathbf{g}$$

$$\nabla \cdot \mathbf{u}_\alpha = 0$$

where, in phase α, $\rho_{\alpha,0}$ is the initial density, $\rho_\alpha(c_i, T)$ is the density with composition c_i and temperature T, $\mathbf{g}$ is the Earth gravity field constant, p_α is the pressure field and μ_α is the dynamic viscosity.

The temperature field is solved using the heat equation with a convective term,

$$\rho c_p\left(\frac{\partial T}{\partial t} + \mathbf{u}_\alpha \cdot \nabla T\right) = k_{th} \nabla^2 T$$

where ρ is the material density, c_p its specific heat capacity, $\mathbf{u}_\alpha$ the velocity field in phase α.

The boundary conditions for chemical transport equations are calculated from the reaction rate. At the metal-slag interface, the aluminothermic reduction $3SiO_2 + 4Al \rightarrow 3Si + 2Al_2O_3$ occurs, this means that positive, respectively negative, flux of Si and Al_2O_3, respectively SiO_2 and Al, have to be considered at the metal-slag interface. Mathematically, those fluxes are considered through Neumann boundary conditions,

$$-D_{Al}\nabla c_{Al} \cdot \mathbf{n} = j_{Al} = -4v_r$$

$$-D_{Si}\nabla c_{Si} \cdot \mathbf{n} = j_{Si} = 3v_r$$

$$-D_{Al_2O_3}\nabla c_{Al_2O_3} \cdot (-\mathbf{n}) = j_{Al_2O_3} = 2v_r$$

$$-D_{SiO_2}\nabla c_{SiO_2} \cdot (-\mathbf{n}) = j_{SiO_2} = -3v_r$$

where v_r is the reaction rate defined as $v_r = k c_{Al}^4 c_{SiO_2}^3 - k' c_{Al_2O_3}^2 c_{Si}^3$ with k and k' the forward and backward kinetic reaction constants, $\mathbf{n}$ the interface normal vector, pointing into metal phase, and c_i the concentration of component i.

The boundary conditions for the Navier-Stokes equations are no slip conditions, i.e. $u_{slag} = 0$ or $u_{metal} = 0$, on every interface except on the metal-slag interface. On the metal-slag interface, denoting $u_{\alpha,r}$ and $u_{\alpha,z}$ the velocities in the radial and vertical direction, the normal velocity is zero on both sides of the interface,

$$u_{\alpha,z} = 0, \qquad \alpha = m, s,$$

The continuity of the radial velocity and tangential stress are ensured by the conditions,

$$u_{m,r} - u_{s,r} = 0 \text{ and}$$

$$\mu_m \partial_z u_{m,r} - \mu_s \partial_z u_{s,r} = 0$$

where μ_α is the dynamic viscosity of phase α.

The heat equation boundary conditions are insulation conditions, i.e. $\nabla T \cdot \mathbf{n} = 0$, for every interface except the metal-slag interface. On the metal-slag interface, the heat flux due to exothermic reaction is considered,

$$j_{th} = v_r \cdot \Delta H_r^0(T)$$

where $\Delta H_r^0(T)$ is the latent heat associated with the aluminothermic reduction at temperature T:

$$\Delta H_r^0(T) = 720680\ [\text{J/mol}] - 133\ [\text{J/mol/K}] \cdot T.$$

3.2.2. *Diffuse interface model*

Due to intensive convection inside the furnace, the interface between slag and metal phases can move,

deform and change its topology, for example by forming droplets of one phase inside the volume of another phase. Therefore, the well-defined interface model, previously described, is not well suited to describe topological changes and a new model considering a diffuse interface could be taken into account to capture the topological interface changes.

A volume averaging method well suits this purpose and is chosen here for the modelling of our two-phase metal-slag liquid system (Whitaker, 1985; Drew & Passman, 1999).

The problem geometry is the same as in the previous section 3.2.1, except that in the volume-averaged representation there is no explicit interface between metal and slag phases. Instead, there is a field of phase fraction. The advantage of this approach is that a highly developed microscopic interface can be modelled as a smooth macroscopic phase transition, which significantly simplifies numerical computations, but requires additional assumptions about the microscopic structure of the system.

One can distinguish a macroscopic interface and a microscopic one. The area A of the microscopic interface contained inside of volume V is replaced, in a volume averaged model, by the field S of the volume density of the area:

$$S = A/V$$

Averaging microscopic transport equation for the molar concentration c_i of component i in phase α gives the following volume-averaged transport equation in terms of intrinsic average concentration $\langle c_i \rangle^\alpha$ (see Appendix A for more details):

$$\frac{\partial}{\partial t}(\varepsilon_\alpha \langle c_i \rangle^\alpha) + \nabla \cdot (\varepsilon_\alpha \langle c_i \rangle^\alpha \langle \mathbf{u}_\alpha \rangle^\alpha - \varepsilon_\alpha D_i \nabla \langle c_i \rangle^\alpha) = S \cdot j_i$$

where j_i is the rate of production of component i in kg/(m^{2}s). Or, omitting the averaging notation, i.e. $\langle \Psi_\alpha \rangle^\alpha \equiv \Psi_\alpha$, we get:

$$\frac{\partial}{\partial t}(\varepsilon_\alpha c_i) + \nabla \cdot (\varepsilon_\alpha c_i \mathbf{u}_\alpha - \varepsilon_\alpha D_i \nabla c_i) = S \cdot j_i$$

The non-conservative form of the above equation:

$$\frac{\partial c_i}{\partial t} + \varepsilon_\alpha \mathbf{u}_\alpha \cdot \nabla c_i + \nabla \cdot (-\varepsilon_\alpha D_i \nabla c_i) = S \cdot j_i + \frac{\partial c_i}{\partial t}(1 - \varepsilon_\alpha) - \frac{\partial \varepsilon_\alpha}{\partial t} c_i$$

In the above equation, the time derivatives on the right-hand side are treated, from the numerical point of view, as source terms. Using a non-conservative form of equation helps to reduce the propagation of numerical errors from the velocity field to the concentration field. On the other hand, however, the global conservation of component i is not guaranteed.

Performing similar averaging operation on the momentum transport equation for each phase, and then assuming a common velocity field $\mathbf{u}$ and pressure p for both phases, gives:

$$\rho_0 \left(\frac{\partial \mathbf{u}}{\partial t} + \mathbf{u} \cdot \nabla \mathbf{u}\right) = -\nabla p + \nabla \cdot \mathbf{K} + \mathbf{f}$$

$$\mathbf{K} = \mu(\nabla \mathbf{u} + (\nabla \mathbf{u})^\top)$$

$$\mathbf{f} = (\rho(c_i, \varepsilon_\alpha) - \rho_0)\mathbf{g}$$

$$\rho(c_i, \varepsilon_\alpha) = \varepsilon_m \rho_m(c_i) + \varepsilon_s \rho_s(c_i)$$

$$\rho_0 = \varepsilon_m \rho_{m,0} + \varepsilon_s \rho_{s,0}$$

$$\mu^{-1} = \varepsilon_m \mu_m^{-1} + \varepsilon_s \mu_s^{-1}$$

where $\mathbf{K}$ is the viscous stress tensor, p is hydrodynamic pressure, $\mathbf{f}$ is the volume density of the body force due to gravity, $\mathbf{g}$ is gravitational acceleration, $\rho_{m,0}$ and $\rho_{s,0}$ are initial densities of metal and slag phases, μ_m and μ_s are constant dynamic viscosities of correspondingly metal and slag phases, $\rho(c_i, \varepsilon_\alpha)$ is the mixture density as a function of phase fraction and components concentrations, ρ_0 is the mixture density as a function of phase fraction only, μ is the mixture dynamic viscosity (fraction-weighted harmonic interpolation). Note that it is assumed here that ρ_0 and μ depend only on slag/metal fraction, and do not depend on components' concentrations c_i, whereas volume force $\mathbf{f}$ depends on both phase fraction and the components concentrations. This is known as the Boussinesq approximation.

The surface tension and Marangoni phenomena are neglected in this problem formulation.

By analogy, the following heat transport equation can be obtained, if we assume a common temperature field T for both phases:

$$(\varepsilon_m \rho_{m,0} c_{p,m} + \varepsilon_s \rho_{s,0} c_{p,s}) \left(\frac{\partial T}{\partial t} + \mathbf{u} \cdot \nabla T\right) + \nabla \cdot (-k \nabla T) = S \cdot j_h$$

$$k^{-1} = \varepsilon_m k_m^{-1} + \varepsilon_s k_s^{-1}$$

$$j_h = \Delta H_R^0(T) \cdot v_R$$

where k is the thermal conductivity of the metal-slag mixture, $c_{p,i}$ is the isobaric specific heat capacity of phase i, indices m and s respectively stand for metal and slag phases, ΔH_R^0 is the standard enthalpy of the reaction of aluminothermic reduction, and v_R is the reaction rate:

$$v_R = \frac{d\xi}{dt}, \qquad \xi = \frac{\Delta n_i}{\nu_i}$$

where ξ is the extent of chemical reaction, Δn_i is the change in the number of moles and ν_i is the stoichiometric coefficient of the i^{th} reactant.

Note that standard rigorous volume averaging procedure gives the *linear* fraction-weighted interpolation for both the thermal conductivity k and the viscosity μ of the metal-slag mixture. Despite that, present model uses *harmonic* fraction-weighted interpolations for k, $k^{-1} = \varepsilon_m k_m^{-1} + \varepsilon_s k_s^{-1}$, and for μ, $\mu^{-1} = \varepsilon_m \mu_m^{-1} + \varepsilon_s \mu_s^{-1}$, which numerically gives less artificial smearing of the diffuse metal-slag interface.

In addition to the bulk equation, boundary

conditions have to be specified. The no-slip boundary condition is imposed on the liquid-crucible interfaces:

$$\mathbf{u} \cdot \boldsymbol{\tau} = 0, \qquad \mathbf{u} \cdot \mathbf{n} = 0$$

where $\boldsymbol{\tau}$ and $\mathbf{n}$ are correspondingly the unit tangent and normal vectors at the interface. A slip and no-penetration boundary conditions are imposed at the liquid-air interface:

$$\mathbf{K} \cdot \mathbf{n} - (\mathbf{n} \cdot \mathbf{K} \cdot \mathbf{n})\mathbf{n} = 0, \qquad \mathbf{u} \cdot \mathbf{n} = 0$$

where $\mathbf{K}$ is the viscous stress tensor. A constant pressure condition ($p = 0$) is at the right bottom corner (in 2D axisymmetric geometry) of the liquid domain. Axial symmetry condition is imposed at the axis of symmetry ($r = 0$).

For the heat transfer equation, thermal insulation is on all the external boundaries of the system. For the species concentration transport equation, the zero flux boundary condition is used at the liquid layer boundaries.

Finally initial conditions have to be set. The initial velocity in the system is zero, initial temperature is 1800 °C. Initial metal composition is pure aluminium. Initial slag composition is 50 wt% of SiO_2 and 50 wt% of CaO.

Table 1. Parameters used in the presented simulations.

Parameters	Value	Unit
Furnace radius, R_f	0.06	m
Slag thickness, H_s	0.05	m
Metal thickness, H_m	0.05	m
Initial temperature, T_0	2073.15	K
Diffusivity of SiO_2 in slag, D_{so}	$1 \cdot 10^{-10}$	m^2/s
Diffusivity of Si in metal, D_s	$2 \cdot 10^{-8}$	m^2/s
Diffusivity of Al_2O_3 in slag, D_{ao}	$1 \cdot 10^{-10}$	m^2/s
Diffusivity of Al in metal, D_a	$2 \cdot 10^{-8}$	m^2/s
Molar mass of CaO, M_{co}	56.0774	g/mol
Molar mass of SiO_2, M_{so}	60.08	g/mol
Molar mass of Al_2O_3, M_{ao}	101.96	g/mol
Molar mass of Al, M_a	26.981539	g/mol
Molar mass of Si, M_s	28.0855	g/mol
Initial mass fraction of CaO, $\omega_{co,0}$	0.5	–
Initial mass fraction of SiO_2, $\omega_{so,0}$	0.5	–
Initial mass fraction of Al_2O_3, $\omega_{ao,0}$	0	–
Initial mass fraction of Al, $\omega_{a,0}$	1	–
Initial mass fraction of Si, $\omega_{s,0}$	0	–
Kinetic coefficient k_{fwd} of the forward reaction $3SiO_2 + 4Al \rightarrow 3Si + 2Al_2O_3$	$1 \cdot 10^{-30}$	$\left(\frac{\text{mol}}{\text{m}^2 \cdot \text{s}}\right) / \left(\frac{\text{mol}}{\text{m}^3}\right)^7$
Kinetic coefficient k_{bwd} of the backward reaction $3SiO_2 + 4Al \leftarrow 3Si + 2Al_2O_3$	$1 \cdot 10^{-22}$	$\left(\frac{\text{mol}}{\text{m}^2 \cdot \text{s}}\right) / \left(\frac{\text{mol}}{\text{m}^3}\right)^5$
Dynamic viscosity of metal, μ_m	$5 \cdot 10^{-4}$	Pa · s
Dynamic viscosity of slag, μ_s	0.09	Pa · s
Thermal conductivity of metal, k_m	108	W/(m · K)
Thermal conductivity of slag, k_s	1.1	W/(m · K)
Specific isobaric heat capacity of metal, $c_{p,m}$	1127	J/(kg · K)
Specific isobaric heat capacity of slag, $c_{p,s}$	1200	J/(kg · K)

4. Results and Discussion

Results for different hypotheses are presented in this section, in order to investigate the effect of different sources of convection. Those sources are density differences due to thermal heterogeneity, density difference due to chemical heterogeneity and forced convection with a velocity imposed on the metal-slag interface. The parameters used in the simulation are presented in Table 1.

4.1. Results with no convection

If no convection is present, the transport of chemical species is only achieved through diffusion. In this case, very long reaction times are found: more than 10 days, as illustrated in Figure 2. The model used for this simulation is the diffuse interface model.

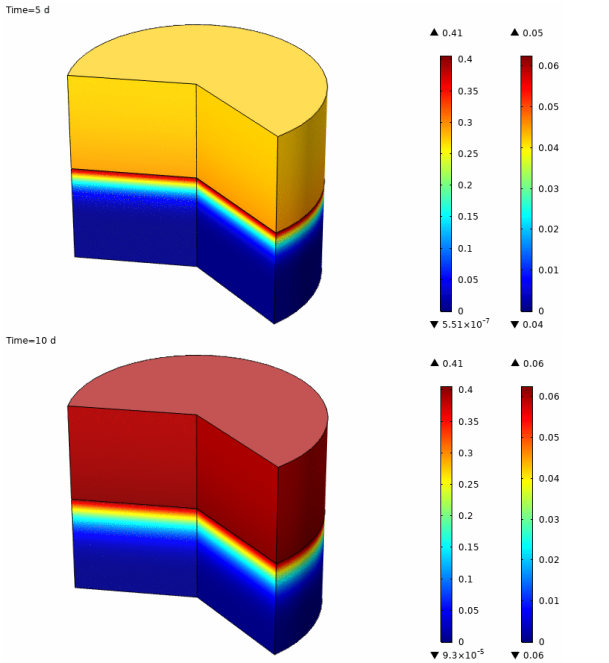

Figure 2. Mole fraction field after 5 days and 10 days in both metal and slag phases resulting from aluminothermic reduction with diffuse interface. The left and right colour bars respectively stand for the Al_2O_3 and Si mole fractions.

4.2. Results with isothermal reaction and natural soluto-gravitational convection

In this section, the results are obtained assuming that the density of the slag and metal does not depend on temperature but only on the chemical composition of phases. The model used for this simulation is the diffuse interface model.

Qualitatively, it appears that the time needed for the reaction to occur is greatly decreased by the effect of the instabilities: as the reaction occurs, the SiO_2 which is heavier than the Al_2O_3 sinks and creates instabilities

which help the transport of the reactants and hasten the reaction. Those instabilities can be seen in Figure 3.

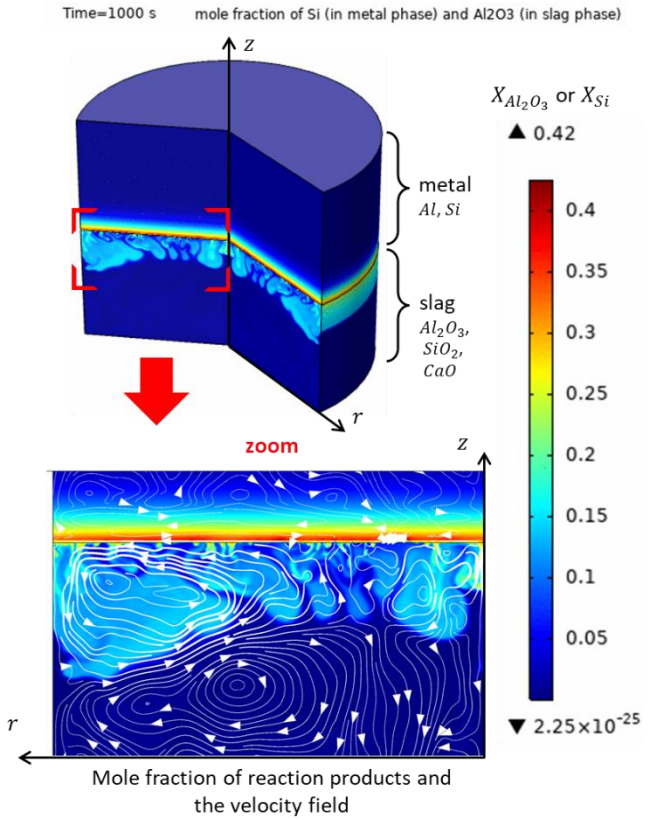

Figure 3. Mole fraction and velocity fields for diffuse interface model with natural soluto-gravitational convection after a reaction time of 1000 s. The represented field is $\varepsilon_m X_{Si} + \varepsilon_s X_{Al_2O_3}$, where ε_m and ε_s respectively denote the volume fraction of metal and slag phases and X_{Si} and $X_{Al_2O_3}$ respectively denote the mole fraction of reaction products Si and Al_2O_3.

4.3. Results with non-isothermal reaction and natural soluto-thermo-gravitational convection

In this section, the results obtained when considering density variations stemming both from temperature and concentration heterogeneities are presented. The model used for this simulation is the diffuse interface model.

To have concentration similar to the previous case in the system, more time is required, as it can be seen in **Figure 4**, when the thermo-gravitational convection is taken into account. As the temperature is higher close to the interface, where the exothermic reaction occurs, and the density is a decreasing function of temperature, the density of the slag in this region is lower which tends to reduce instabilities of the interface and thus reduces the convection at its neighbourhood.

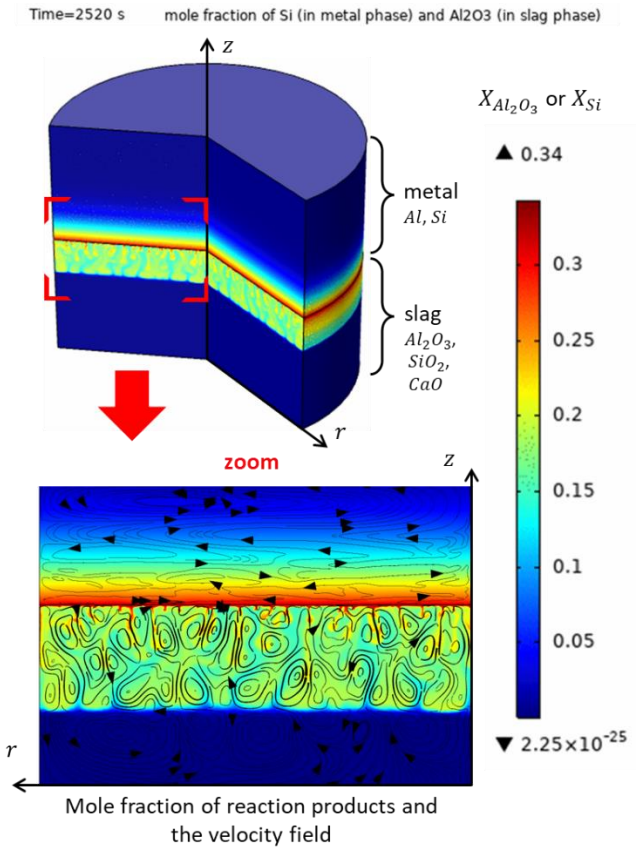

Figure 4. Mole fraction and velocity fields for diffuse interface model with natural soluto- and thermo-gravitational convection after a reaction time of 2520 s. The represented field is $\varepsilon_m X_{Si} + \varepsilon_s X_{Al_2O_3}$ where ε_m and ε_s respectively denote the volume fraction of metal and slag phases and X_{Si} and $X_{Al_2O_3}$ respectively denote the mole fraction of reaction products Si and Al_2O_3.

4.4. Non-isothermal reaction with forced convection

The forced convection is studied by prescribing a velocity on the metal-slag interface, as shown in **Figure 5**. The associated concentration after a 1000 s reaction time is presented in **Figure 6**. The model used for this simulation is the well-defined interface model since, as the velocity is imposed on the metal-slag interface the diffuse interface would be highly disturbed, making the numerical resolution too computationally expensive.

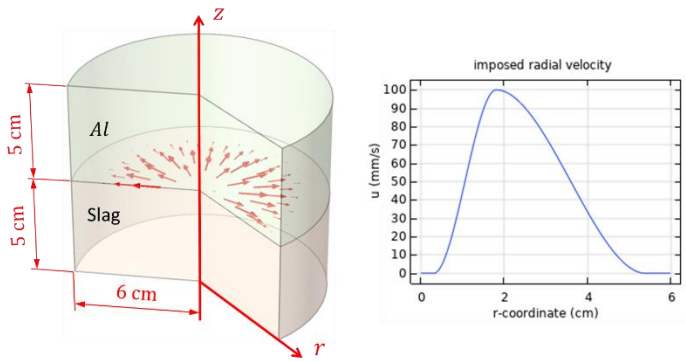

Figure 5. Shape of the velocity field imposed at the metal-slag interface.

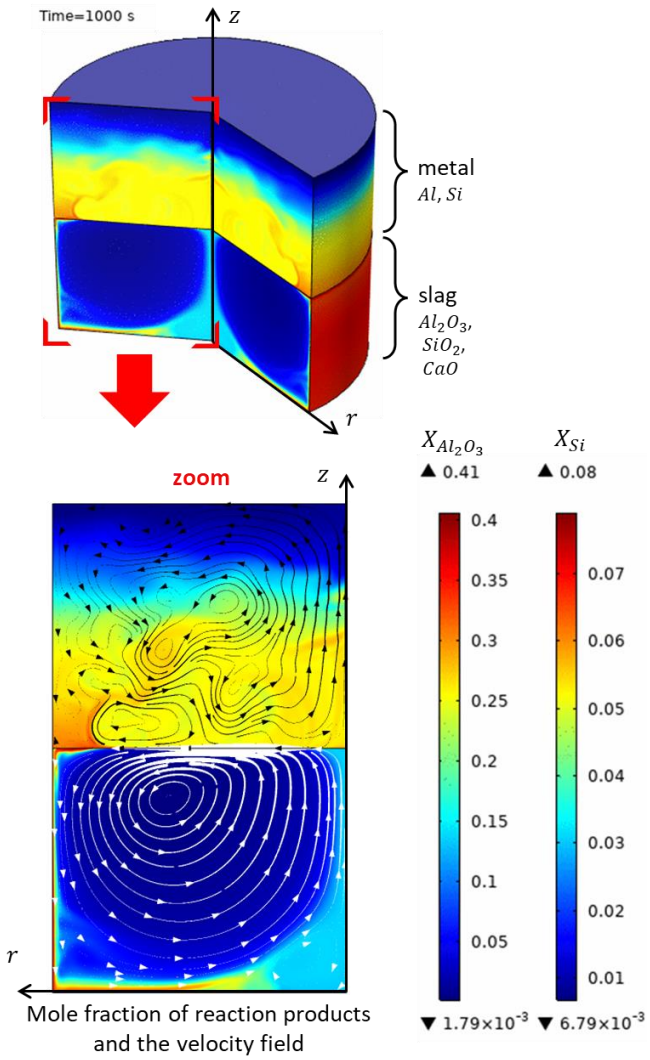

Figure 6. Mole fraction and velocity fields from the well-defined interface model with forced convection at the metal-slag interface, after a reaction time of 1000 s. Two colour scales are used: the left one stands for mole fraction of Al_2O_3 in slag and the right one stands for Si mole fraction in metal.

4.5. Results comparison

A critical point for the aluminothermic reduction process is the kinetics of the reaction: a quicker reaction requires less energy to be spent to keep the system melted.

Consideration of density difference caused by composition accelerates the reaction process, while introducing also thermo-gravitational convection reduced the reaction process by stabilizing the interface. Those results can be seen in **Figure 7**. Forced convection appears also as rising strongly the reaction rate. The importance of considering convection phenomena is proven by the model where no convection is considered: in this case the reaction is far slower than in the three other models with convection.

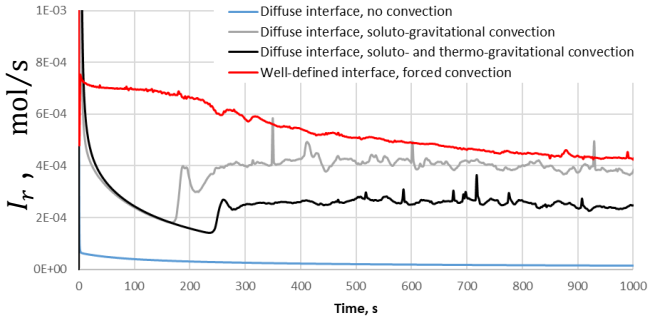

Figure 7. Global reaction rate I_r comparison between different numerical models.

5. Conclusions

Thanks to a separate consideration of each component of the transport phenomena in the numerical model, we have successfully estimated the impact of each one on the global reaction rate. Models demonstrate a crucial importance of the slag and metal stirring for the process of aluminothermic reduction of quartz. To optimize the process, a major interest on the stirring should be taken into account.

In this numerical study the stirring has been modelled by prescribing a velocity on the metal-slag interface. This is the first step into investigating other forms of stirring. Future studies could be focussed, for instance, on the stirring provoked by gas injection.

Funding

The work presented has been developed in the framework of the SisAl Pilot project. This project has received funding from the European Union's Horizon 2020 research and innovation program under Grant Agreement No. 869268.

Appendix A: volume averaging theory

The application of volume averaging transforms exact microscopic transport equations into volume-averaged macroscopic equations expressed in terms of volume-averaged fields. Let us introduce two types of volume-averaged fields: the superficial one and the intrinsic one.

The superficial average of a microscopic field Ψ is represented by the following formula:

$$\langle \Psi_\alpha \rangle = \frac{1}{V_0} \int_{V_0} \Psi Y_\alpha dV$$

where V_0 is a representative volume, over which an averaging is performed at every point in space, subscript $\alpha = m, s$ indicates the metal or slag phase, and Y_α is the phase indicator function:

$$Y_\alpha = \begin{cases} 1, & \text{in phase } \alpha \\ 0, & \text{elsewhere} \end{cases}$$

Choosing $\Psi = 1$ gives the volume fraction ε_α of phase α:

$$\varepsilon_\alpha = \frac{1}{V_0}\int_{V_0} Y_\alpha dV = \frac{V_\alpha}{V_0}$$

where V_α is the volume of α-phase in V_0. Note that $\sum_\alpha V_\alpha = V_0$ and $\sum_\alpha \varepsilon_\alpha = 1$. The intrinsic average of a microscopic field Ψ is given by:

$$\langle \Psi_\alpha \rangle^\alpha = \frac{1}{V_\alpha}\int_{V_0} \Psi Y_\alpha dV = \frac{1}{\varepsilon_\alpha}\langle \Psi_\alpha \rangle$$

In terms of these quantities, the two following theorems constitute the basis for averaging of microscopic transport equations (Whitaker, 1985; Drew & Passman, 1999):

- Gauss rule:

$$\varepsilon_\alpha \langle \nabla \Psi_\alpha \rangle^\alpha = \nabla(\varepsilon_\alpha \langle \Psi_\alpha \rangle^\alpha) + S \cdot \overline{\mathbf{n}_\alpha \Psi_\alpha}$$

- Leibniz rule

$$\frac{\partial}{\partial t}(\varepsilon_\alpha \langle \Psi_\alpha \rangle^\alpha) = \varepsilon_\alpha \left\langle \frac{\partial \Psi_\alpha}{\partial t} \right\rangle^\alpha + S \cdot \overline{\Psi_\alpha(\mathbf{u}_\Gamma \cdot \mathbf{n}_\alpha)}$$

where S is the volume density of the interfacial area in m^2/m^3, $\mathbf{n}_\alpha$ is the unit normal vector at the interface pointing out of the α-phase, and $\mathbf{u}_\Gamma$ is the microscopic velocity of the interface itself, whereas overbar $\overline{\Psi}$ denotes averaging over the interface.

The following hypotheses are also made: the diffusion coefficients are assumed to be constant, $D_i = const$; the concentration at the interface equals its intrinsic average value $c_i|_\Gamma = \langle c_i \rangle^\alpha$; the dispersive terms are neglected, $\langle c_i \mathbf{u}_\alpha \rangle^\alpha = \langle c_i \rangle^\alpha \langle \mathbf{u}_\alpha \rangle^\alpha$.

In order to know the value of the volume density S of the interfacial area, one needs a particular model for the macroscopic S_{macro} and the microscopic S_{micro} volume densities of interfacial areas.

The above stated Gauss rule for function $\Psi = 1$ gives us the amount of the macroscopic interface:

$$\nabla \varepsilon_\alpha = -S \cdot \overline{\mathbf{n}}_\alpha \quad \Rightarrow \quad |\nabla \varepsilon_\alpha| = S_{macro}$$

because integrating this quantity over the system volume V gives exactly the amount of macroscopic interfacial area A:

$$\int_V S_{macro} dV = \int_V |\nabla \varepsilon_\alpha| dV = A$$

In case of a uniform fraction field $\varepsilon_\alpha \approx const$, there is no macroscopic interface:

$$\varepsilon_\alpha \approx const \quad \Rightarrow \quad S_{macro} = |\nabla \varepsilon_\alpha| \approx 0$$

However, there is a microscopic interface to be considered. Let us assume a constant diameter $D_d \approx const$ of dispersed phase droplets. Then, based on simple geometric calculation in a 3D geometry we get:

$$S_{micro} = \frac{6\varepsilon_d}{D_d}$$

where ε_d is the volume fraction of the dispersed phase.

The symmetric model is often used when both phases can be potentially the dispersed ones, depending on their volume fraction:

$$S_{micro} = \frac{6\varepsilon_d(1-\varepsilon_d)}{D_d}$$

In total we get:

$$S = S_{macro} + S_{micro} = |\nabla \varepsilon_\alpha| + \frac{6\varepsilon_d(1-\varepsilon_d)}{D_d}$$

References

Amini, S. H. (2005). Dissolution rate and diffusivity of lime in steelmaking slag and development of fluoride-free fluxes, PhD thesis.

Bruzzone, A. G., Sinelshikov, K., Cepolina, E., Giovannetti, A., & Pernas, J. (2021). Autonomous systems for industrial plants and iron & steel facilities. Proceedings of the 33rd European Modeling & Simulation Symposium (EMSS 2021), (pp. 418-422).

Deqing, W., & Ziyuan, S. (2001). Aluminothermic reduction of silica for the synthesis of alumina-aluminum-silicon composite. Journal of Materials Synthesis and Processing, 9(5), 241-246.

Doering, C. R. (2020). Turning up the heat in turbulent thermal convection. Proceedings of the National Academy of Sciences, 117(18), 9671–9673.

Drew, D. A., & Passman, S. L. (1999). Theory of multicomponent fluids, Applied mathematical sciences (Vol. 135). New York: Springer.

Du, Y., Chang, Y., Huang, B., Gong, W., Jin, Z., Xu, H., . . . Xie, F.-Y. (2003). Diffusion coefficients of some solutes in fcc and liquid Al: critical evaluation and correlation. Materials Science and Engineering: A, 363(1-2), 140–151.

Fang, D.-L., Zhao, Y.-C., Wang, S.-S., Hu, T.-S., & Zheng, C.-H. (2020). Highly efficient synthesis of nano-Si anode material for Li-ion batteries by a ball-milling assisted low-temperature aluminothermic reduction. Electrochimica Acta, 330, 135346.

Gao, S., Yang, D., Pan, Y., Geng, L., Li, S., Li, X., . . . Yang, H. (2019). From natural material to high-performance silicon based anode: Towards cost-efficient silicon based electrodes in high-performance Li-ion batteries. Electrochimica Acta, 327, 135058.

Jiang, K., Chen, Z., Ma, W., Cao, S., Zhang, H., & Zhu, Y. (2021). Effect of Carbonaceous Reducers on Carbon Emission during Silicon Production in SAF of 8.5 MVA and 12.5 MVA. Silicon, 1–11.

Liu, X., Lu, J., Jiang, J., Jiang, Y., Gao, Y., Li, W., . . . Zhang, J. (2021). Enhancing lithium storage performance by strongly binding silicon

nanoparticles sandwiching between spherical graphene. Applied Surface Science, 539, 148191.

Mirjalili, S., Jain, S. S., & Dodd, M. (2017). Interface-capturing methods for two-phase flows: An overview and recent developments. Center for Turbulence Research Annual Research Briefs, 2017(117-135), 13.

Mishra, K., Zheng, J., Patel, R., Estevez, L., Jia, H., Luo, L., . . . Zhang, J.-G. (2018). High performance porous Si@C anodes synthesized by low temperature aluminothermic reaction. lectrochimica Acta, 269, 509-516.

Park, J., Sridhar, S., & Fruehan, R. J. (2014). Kinetics of reduction of SiO2 in SiO2-Al 2O3-CaO slags by Al in Fe-Al(-Si) melts. Metallurgical and Materials Transactions B, 45, 1380-1388.

Philipsson, H., Wallin, M., Einarsrud, K. E., & Tranell, G. (2021). Kinetics of Silicon Production by Aluminothermic Reduction of Silica Using Aluminum and Aluminum Dross as Reductants. In A. N. Waernes, G. Tranell, M. Tangstad, E. Ringdalen, & C. van der Eijk (Ed.), Proceedings of the 16th International Ferro-Alloys Congress (INFACON XVI) (pp. 1-10). Trondheim, Norway: SINTEF/NTNU/FFF.

Pizzini, S. (1984). Solar grade silicon versus electronic grade silicon for photovoltaic applications. Journal of power sources, 11(1-2), 115-118.

Prabriputaloong, K., & Piggot, M. R. (1973). Reduction of SiO2 by Molten Al. Department of Chemical Engineering, University of Toronto, Toronto, Ontario, Canada, 184-185.

Ramaekers, K., Pollaris, H., & Claes, L. (2014). Analysing and optimising a dual resource constraint production system using simulation. Proceedings of the International Conference on Modeling and Applied Simulation, (pp. 54-59). Bordeaux, France.

Roberts, S., & Dobson, P. (1984). Evidence for reaction at the AI-SiO, interface. J. Phys. D: Appl. Phys., 14.

Talako, T. L., Yakovleva, M. S., Astakhov, E. A., & Letsko, A. I. (2018). Structure and properties of detonation gun sprayed coatings from the synthesized FeAlSi/Al2O3 powder. Surface and Coatings Technology, 353, 93-104.

Tkadleckova, M. (2021). Numerical Modelling in Steel Metallurgy. Metals, 11(6), 885.

Whitaker, S. (1985). A simple geometrical derivation of the spatial averaging theorem. Chemical engineering education, 19, 18–52.

Zhang, J., Si, Y., Leng, C., & Yang, B. (2016). Molecular dynamics simulation of Al-SiO2 sandwich nanostructure melting and low-temperature energetic reaction behavior. RSC advances, 6(64), 59313-59318.